



Short communication

Fabrication of SOFCs on Ni/NiAl₂O₄ support

Anuwat Srisuwan^{a,*}, Darunee Wattanasiriwech^a, Suthee Wattasiriwech^a, Pavadee Aungkavattana^b

^aSchool of Science, Mae Fah Luang University, Muang, Chiang Rai 57100, Thailand

^bNational Metal and Materials Technology Center, Pathumthani, 12120, Thailand



HIGHLIGHTS

- Preparation and properties of Ni/NiAl₂O₄ composites were studied to use as an SOFC support.
- Ohmic resistance of Ni/NiAl₂O₄ supports are improved with higher Ni content.
- Densification of YSZ electrolyte layer is controlled by firing rate during sintering process.
- Crack and pore on electrolyte suppress the OCV of cell performance.

ARTICLE INFO

Article history:

Received 13 September 2013

Received in revised form

11 November 2013

Accepted 12 November 2013

Available online 20 November 2013

Keywords:

Fuel cell

External support

Firing rate

Cell performance

ABSTRACT

NiO/NiAl₂O₄ composites with 50/50, 55/45 and 60/40 wt.%/wt.% ratios were prepared from Al₂O₃ and NiO powders to use as an external SOFC supports that were denoted as 50NO50NS, 55NO45NS and 60NO40NS, respectively. Effects of support compositions and firing rates for sintering and reduction on shrinkage, thermal expansion coefficient and electrical conductivity of the supports were studied. The cells with NiO/NiAl₂O₄//Ni-YSZ//YSZ//Pt configuration were co-sintered at 1400 °C in air and reduced at 800 °C in H₂ by varying the firing rate of 1 °C min⁻¹ (coded as -1) and 3 °C min⁻¹ (coded as -3). A dense YSZ electrolyte was observed in 50NO50NS-3 and 55NO45NS-3 cells, while cracks and pores appeared in the YSZ layer for 60NO40NS-3 cell indicating the greater difference in shrinkage and TEC between 60NO40NS support and YSZ electrolyte. Crack formation was eliminated and a dense YSZ electrolyte was obtained when the firing rate was reduced to 1 °C min⁻¹, suggesting that the different shrinkage between supports and YSZ electrolyte during sintering process can be alleviated at this firing rate. The highest power density (106 mW cm⁻² at 800 °C) was thus obtained for 60NO40NS-1 cell due to a superior electrical conductivity of 60NO40NS support to 50NO50NS and 55NO45NS.

© 2013 Elsevier B.V. All rights reserved.

1. Introduction

Solid oxide fuel cells (SOFCs) have been widely suggested as an electrochemical device that provides energy efficiency and clean power generation [1]. SOFCs are a complex electrochemical device composed of porous cathode, porous anode and dense electrolyte [2]. In cell fabrication, one of the components such as electrolyte, anode or cathode is selected to use an internal support [3]. However, it was found that the large thickness of the internal support also produced ohmic polarization loss resulting in the deterioration of cell performance [4].

Recently the electronic conducting materials with a porous structure have been studied to use as an external support so thin

electrolyte and electrode layers can be fabricated. For example, ferrochromium metal (FeCr) was selected because of its high strength and high electronic conductivity [5,6]. However, the large particles of the commercial grade FeCr powder ($\sim 10\text{--}30 \mu\text{m}$) resulted in surface pores after forming, fabrication of dense electrolyte on this support was thus required a complex apparatus. Besides, the austenite second phase was formed due to the inter-diffusion between FeCr support and the Ni-YSZ anode during sintering process [7]. The much greater thermal expansion coefficient (TEC) of the austenite phase ($19\text{--}20 \times 10^{-6} \text{ K}^{-1}$) to that of YSZ electrolyte ($10 \times 10^{-6} \text{ K}^{-1}$) led to cracking of the layers. Exploration for a suitable material is still highly required [8,9]. Among various materials, Ni metal is an attractive choice because it has excellent electronic conductivity and high catalytic activity. However, the thermal expansion coefficient of pure Ni metal ($16 \times 10^{-6}/\text{K}$) is much higher than that of Ni-YSZ anode ($12 \times 10^{-6}/\text{K}$) and YSZ electrolyte so cracks are generated during cell operation [10].

* Corresponding author.

E-mail address: anuwat.srisuwan@gmail.com (A. Srisuwan).

Compositing Ni with a ceramic such as NiAl_2O_4 can be an attractive choice because NiAl_2O_4 phase has high strength while Ni has high electronic and catalytic activity. It was reported that electronic conductivity of the reduced $\text{NiO}/\text{NiAl}_2\text{O}_4$ composite was greatly improved when NiO ratio was over 40 wt.% [11]. Although the electronic conductivity of the reduced $\text{NiO}/\text{NiAl}_2\text{O}_4$ composite was improved with increasing NiO phase, an increase of NiO phase resulted in the higher thermal expansion coefficient due to the transformation of NiO to Ni metallic phase. The difference of TEC values between the $\text{Ni}/\text{NiAl}_2\text{O}_4$ support and other cell components could possibly result in internal stress and finally failure after operation.

This paper aimed to study $\text{NiO}/\text{NiAl}_2\text{O}_4$ composites as a support for SOFC. Effects of firing rate on shrinkage and TEC of the supports and cell components on densification of YSZ electrolyte was studied. Electrical conductivity of the supports was measured to consider the ability of electron movement during cell performance.

2. Experimental procedure

2.1. $\text{NiO}/\text{NiAl}_2\text{O}_4$ characterization and properties

$\text{NiO}/\text{NiAl}_2\text{O}_4$ composite was prepared from Al_2O_3 (purchased by Cernic International Co., Thailand) and NiO (purchased by American Elements, USA) powders and the average particle sizes (D (4.3)) of Al_2O_3 and NiO powders were about 3.31 and 5.75 μm , respectively. Al_2O_3 and NiO powders were mixed at weight ratios of 29/71, 26/74, 23/77 using a vibrational milling in a polypropylene jar and TZP grinding balls for 20 min. Water was used as a dispersing medium while 2 wt.% PVA (Poly-vinyl alcohol) was used as a binder. After overnight drying in a hot-air oven, the mixed powder was sieved through a 200-mesh stainless steel sieve and uniaxially pressed into 15 mm-diameter pellets using a stainless steel die. The green pellets were subsequently sintered in an electrical furnace at 1400 °C for 1 h in order to obtain the NiAl_2O_4 phase while the excess NiO remained as an oxide phase. The weight ratios of $\text{NiO}/\text{NiAl}_2\text{O}_4$ were 50/50, 55/45 and 60/40 and the samples were coded as 50NO50NS, 55NO45NS and 60NO40NS, respectively.

All sintered 50NO50NS, 55NO45NS and 60NO40NS samples were subsequently fired at 800 °C in H_2 atmosphere at a flow rate of 20 $\text{cm}^3 \text{min}^{-1}$ in order to reduce the NiO phase to Ni metal. These supports were denoted as R50NO50NS, R55NO45NS and R60NO40NS, respectively. Phase composition of the $\text{NiO}/\text{NiAl}_2\text{O}_4$ samples both before and after reduction was identified using an X-ray diffractometer (PANalytical, X'Pert PRO MPD) with $\text{Cu-K}\alpha$ radiation. Apparent porosity of all supports was measured based on the Archimedes' principle. Microstructures of the reduced $\text{NiO}/\text{NiAl}_2\text{O}_4$ samples were examined using a scanning electron microscope (JEOL, JSM-5410LV) in the back-scattered electron mode (BSE). The shrinkage of cell

components was measured in air in 2 steps at the pre-sintering temperature range (25–1100 °C) and at the sintering temperature range (1100–1400 °C). The shrinkage difference (ΔS) was calculated for the purpose of compatibility study of cell components during co-sintering process. Thermal expansion coefficients were measured by a dilatometer (NETZSCH, DIL 402C) in the temperature range from 100 °C to 800 °C in N_2 atmosphere. The bar shaped samples with a dimension of 4 mm × 9 mm × 1 mm were prepared for electrical conductivity measurement by the DC-four probe method under H_2 atmosphere using Pt wire as a current collector.

2.2. Cell fabrication and performance

The SOFC with a configuration of $\text{Ni-YSZ}/\text{YSZ}/\text{Pt}$ was fabricated on 50NO50NS, 55NO45NS and 60NO40NS supports. $\text{NiO}/\text{NiAl}_2\text{O}_4$ powder was prepared into 15-mm diameter pellets and then pre-sintered at 1100 °C for 1 h in air. The Ni-YSZ anode slurry was prepared by mixing Ni-YSZ composite powder (50/50 wt.%/wt.%, D (4.3) ~5.27 μm , purchased by American Elements, USA) with terpenol using the weight ratio of 70/30. The Ni-YSZ slurry was applied on one side of the $\text{NiO}/\text{NiAl}_2\text{O}_4$ pellets by a screen printing method and pre-sintering at 1100 °C for 1 h in air. Yttria-stabilized zirconia (YSZ) electrolyte slurry was prepared by dispersing the YSZ powder (D (4.3) ~0.24 μm , TOSHO Corporation, Japan) in ethanol at the concentration of 10 g L^{-1} . The electrolyte slurry was deposited on the Ni-YSZ layer by the electrophoretic deposition method (EPD) with the applied DC voltage of 20 V for 30 s. The $\text{NiO}/\text{NiAl}_2\text{O}_4/\text{Ni-YSZ}/\text{YSZ}$ configurations were co-sintered at 1400 °C for 1 h. To study the effect of firing rate on microstructure of the cells, the firing rate of 1 °C min^{-1} and 3 °C min^{-1} were used during sintering and reduction. Pt cathode was applied on the sintered samples using a screen printing technique with the active cathode area about 63.62 mm^2 . It was then co-fired at 1050 °C for 1 h in air. Fig. 1 shows the set-up for cell performance measurement. The cell was attached to alumina tube using a pyrex glass ring as a sealant. Pt mesh and wire were attached to the $\text{NiO}/\text{NiAl}_2\text{O}_4$ support and Pt cathode side in order to use as the current collector. The cell was heated up to 840 °C for 1 h to melt the pyrex glass. H_2/O_2 as fuel/oxidant was fed into the porous $\text{NiO}/\text{NiAl}_2\text{O}_4$ support and cathode sides, respectively. The flow rate of both gases was constantly applied at 20 $\text{cm}^3 \text{min}^{-1}$. The codes for single cells with parameter variations are shown in Table 1. Current (I)–voltage (V) characteristics of the cells at 800 °C was measured through an electronic load.

3. Results and discussion

3.1. $\text{NiO}/\text{NiAl}_2\text{O}_4$ characterization

Fig. 2 shows XRD patterns of the 50NO50NS support after sintering and reduction. After sintering at 1400 °C in air, all supports

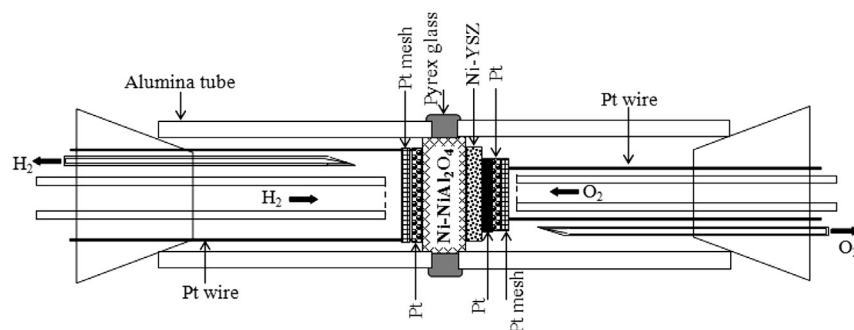


Fig. 1. The single cell testing set up.

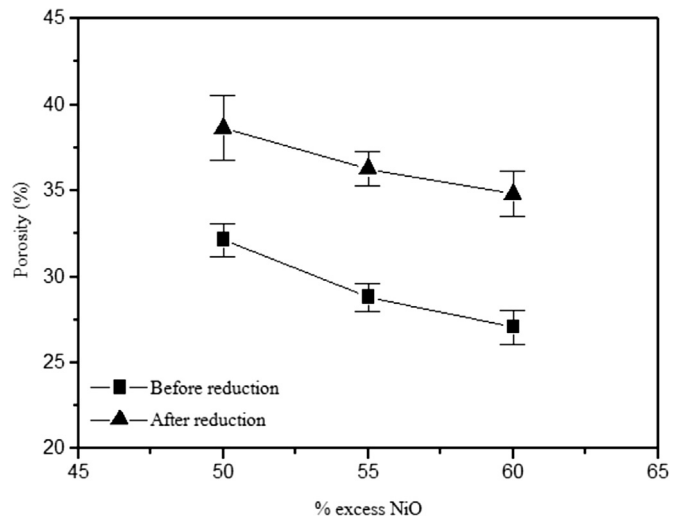
Table 1

Firing rate conditions of the cells during sintering and reduction.

Composition of support (wt.%)		Firing rate ($^{\circ}\text{C min}^{-1}$)	Codes
NiO	NiAl ₂ O ₄		
50	50	1	50NO50NS-1
55	45	1	55NO45NS-1
60	40	1	60NO40NS-1
50	50	3	50NO50NS-3
55	45	3	55NO45NS-3
60	40	3	60NO40NS-3

showed the presence of NiAl₂O₄ phase while the Al₂O₃ phase was not detected anymore. This indicated a complete reaction between NiO and Al₂O₃. The excess NiO could also be detected. XRD patterns of 50NO50NS support after reduction at 800 °C in H₂ confirmed that NiO was completely transformed into Ni metallic phase. The phase transformation for 55NO45NS and 60NO40NS supports after sintering and reduction was similar to that of 50NO50NS support. Therefore, this reduction method of 800 °C for 1 h in H₂ was applied to convert NiO phase into Ni phase before cell performance test.

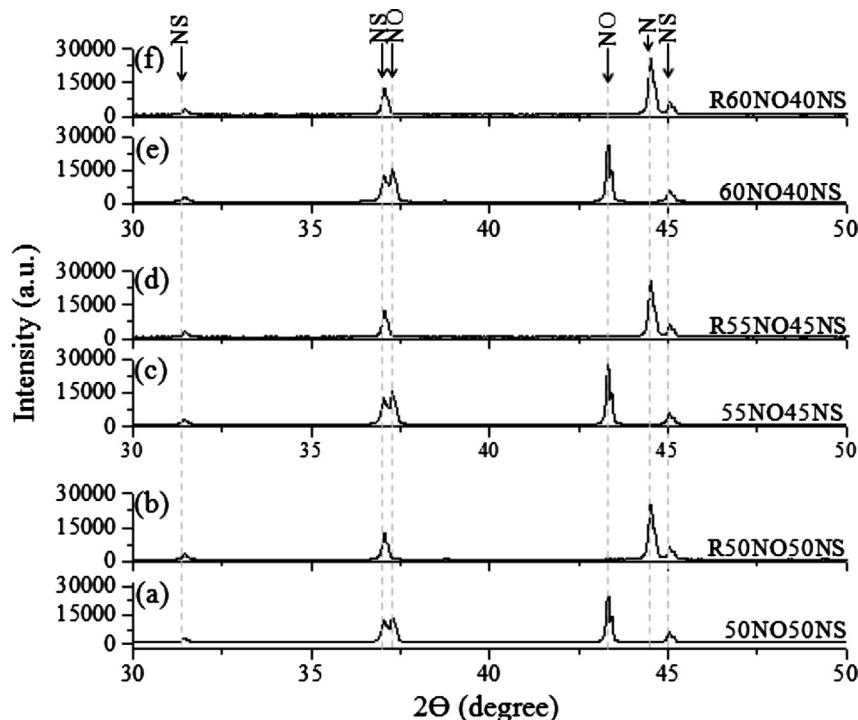
Porosity of 50NO50NS, 55NO45NS and 60NO40NS supports after sintering at 1400 °C in air determined by the Archimedes method is shown in Fig. 3. The porosity of the sintered 50NO50NS support was about 32% and decreased when NiO proportion was increased in 55NO45NS support. This result occurred because NiO had lower melting point than NiAl₂O₄ [12]. Higher NiO proportion was significantly caused to increase densification on NiO/NiAl₂O₄ supports. The lowest porosity of about 27% was thus found for the sintered 60NO40NS support. After reduction, the porosity of the R50NO50NS, R55NO45NS and R60NO40NS supports (Fig. 3) was increased to 39%, 36% and 35%, respectively. It was evidenced to confirm development of porosity after reduction of the supports. The change of porosity in NiO/NiAl₂O₄ supports could be explained that oxygen ions in NiO phase was induced by H₂ gas to form steam

Fig. 3. Porosity of various NiO/NiAl₂O₄ supports before and after reduction.

while NiO phase was converted into Ni metallic phase [13]. An increase of pore volume in all supports was sufficient to facilitate the transport of reactant and product gases [14].

Fig. 4 presents the BSE-SEM micrographs of the Ni/NiAl₂O₄ supports. Ni and NiAl₂O₄ phases could be distinguished by the different atomic numbers. Heavier Ni atoms appeared as high brightness while NiAl₂O₄ appeared as the gray color phase. The connection of the Ni phase was significantly increased with increasing NiO content.

The electrical conductivity of Ni/NiAl₂O₄ supports with different Ni contents is graphically shown in Fig. 5. It could be seen that all supports had the metallic behavior by a decrease in the electrical

Fig. 2. X-ray diffraction patterns of (a, c, e) NiO/NiAl₂O₄ after sintering at 1400 °C in air and (b, d, f) Ni/NiAl₂O₄ after reduction at 800 °C for 1 h in H₂ (NO=NiO, NS=NiAl₂O₄ and Ni=Ni).

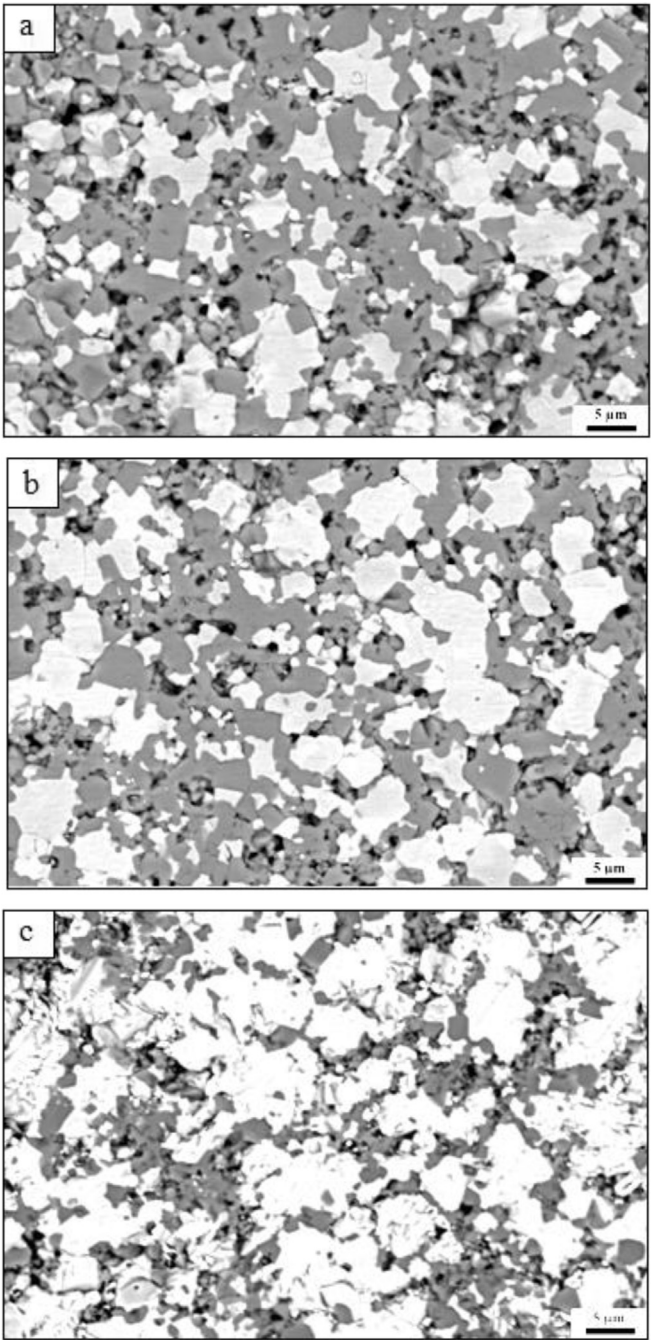


Fig. 4. Back-scattered SEM micrographs of (a) R50NO50NS, (b) R55NO45NS and (c) R60NO40NS supports.

conductivity with increasing measuring temperature. The electrical conductivity of the supports was greatly depended on the excess NiO content. An increase in the electrical conductivity of the supports was observed with higher Ni metallic connection. The highest electrical conductivity (1517 S cm^{-1}) was thus found in the R60NO40NS supports which mainly contributed to an increase of the Ni electronic conductor fraction. In all cases, the supports had electrical conductivity $>1000 \text{ S cm}^{-1}$ indicating the metallic type conductivity [15].

Shrinkage and TEC values of the cell components are shown in Tables 2 and 3, respectively. Both properties are important for the cell fabrication because high different shrinkage and TEC values of

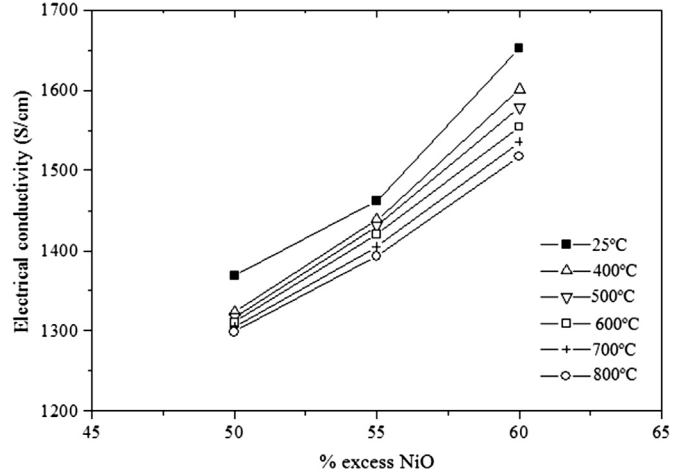


Fig. 5. Electrical conductivity of Ni/NiAl₂O₄ supports measured at different temperatures.

the supports with other cell components could result in the bending and cracking of the support during co-sintering and reduction process. All supports had the shrinkage values in the range of pre-sintering process (25–1100 °C) close to those of YSZ electrolyte and Ni-YSZ anode which was observed both in the firing rate of $1 \text{ }^{\circ}\text{C min}^{-1}$ and $3 \text{ }^{\circ}\text{C min}^{-1}$. Shrinkage difference (ΔS) of the samples between pre-sintering and sintering steps was calculated to understand the shrinkage behavior of supports and other cell components after pre-sintering step. Shrinkage difference of electrolyte, anode and supports were in close values. Exception was found in the 60NO40NS support with the firing rate of $3 \text{ }^{\circ}\text{C min}^{-1}$ which had the greatest difference as compared to the YSZ electrolyte and the Ni-YSZ anode, so pores could be formed on YSZ electrolyte during sintering process. This implied the maximum NiO content in the support.

Although porosity of support was decreased with increasing NiO content, the porosity values of all supports were sufficient for gas permeability. An increase of NiO ($>60 \text{ wt.\%}$) was a cause of the different TEC value between the support and electrolyte which resulted in the crack generation. It was implied that the optimum NiO content should not higher than 60 wt.%.

3.2. Microstructures and performance of Ni/NiAl₂O₄ supported cells

Fractured surface and surface of 50NO50NS-3, 55NO45NS-3 and 60NO40NS-3 cells are shown in Figs. 6 and 7, respectively. Good adhesion of the layers in the 50NO50NS-3 (Fig. 6a), 55NO45NS-3 cells (Fig. 6b) and 60NO40NS-3 (Fig. 6c) was observed. Thickness of YSZ electrolyte and Ni-YSZ anode layer was about 5 μm. Fig. 7a and b confirmed that high densification of YSZ electrolyte was obtained for 50NO50NS-3 and 55NO45NS-3 cells because of the similar shrinkage difference and TEC of 50NO50NS and 55NO45NS to other cell components. In contrast, pores and cracks in the YSZ electrolyte layer were found in the 60NO40NS-3 cell, as shown in Fig. 7c. Generation of the defects could significantly relate to the shrinkage difference and TEC during sintering and reduction. The mismatch in shrinkage difference between 60NO40NS support and YSZ electrolyte during co-sintered process with the firing rate of $3 \text{ }^{\circ}\text{C min}^{-1}$ (Table 2) affected on the poorly sintered densification of YSZ electrolyte layer. In cracking defect, it could be explained that high different TEC values of 60NO40NS support and YSZ electrolyte could produce stress during reduction which led to the generation of crack on YSZ electrolyte film for 60NO40NS-3 cell. This problem

Table 2

The shrinkage values of cell components with different firing rate.

Samples	Shrinkage (%) ($3\text{ }^{\circ}\text{C min}^{-1}$)		ΔS	Shrinkage (%) ($1\text{ }^{\circ}\text{C min}^{-1}$)		ΔS
	25–1100 $^{\circ}\text{C}$	1100–1400 $^{\circ}\text{C}$		25–1100 $^{\circ}\text{C}$	1100–1400 $^{\circ}\text{C}$	
YSZ	6.07 ± 0.60	16.81 ± 0.31	10.74	8.11 ± 0.73	18.22 ± 0.17	10.11
Ni-YSZ	6.19 ± 0.48	17.16 ± 0.14	10.97	8.24 ± 0.15	18.42 ± 0.39	10.18
50NO50NS	6.08 ± 0.21	16.50 ± 0.48	10.42	9.08 ± 0.35	19.25 ± 0.12	10.17
55NO45NS	6.43 ± 0.10	18.42 ± 0.65	11.93	9.45 ± 0.28	20.55 ± 0.45	11.10
60NO40NS	6.95 ± 0.37	20.17 ± 0.41	13.22	9.96 ± 0.46	21.82 ± 0.27	11.86

Table 3

The thermal expansion coefficient values of the cell component measured at $100\text{ }^{\circ}\text{C}$ – $800\text{ }^{\circ}\text{C}$.

Samples	Thermal expansion coefficient (K^{-1})	Ref.
YSZ	10.1×10^{-6}	[12]
Ni-YSZ	12.4×10^{-6}	[13]
R50NO50NS	10.5×10^{-6}	This work
R55NO45NS	11.3×10^{-6}	This work
R60NO40NS	12.3×10^{-6}	This work

was solved by reducing the firing rate from $3\text{ }^{\circ}\text{C min}^{-1}$ to $1\text{ }^{\circ}\text{C min}^{-1}$ during sintering and reduction processes. Fractured surface and surface of 50NO50NS-1, 55NO45NS-1 and 60NO40NS-1 cells are shown in Figs. 8 and 9, respectively. The shrinkage difference between the supports and YSZ electrolyte was compatible for the firing rate of $1\text{ }^{\circ}\text{C min}^{-1}$ so higher densification of YSZ layer was

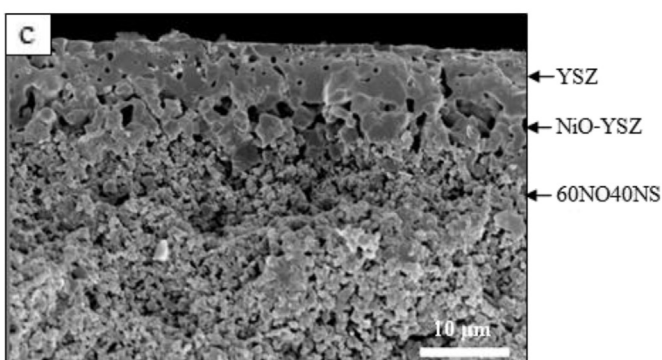
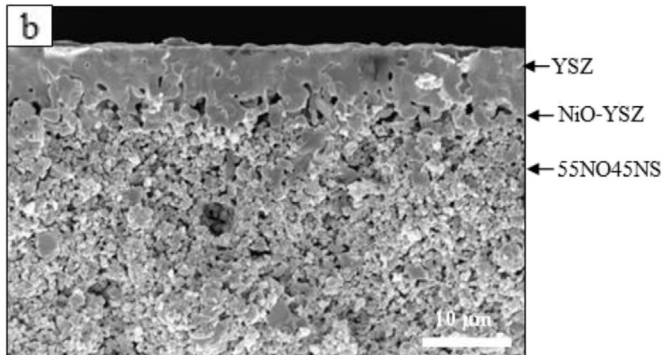
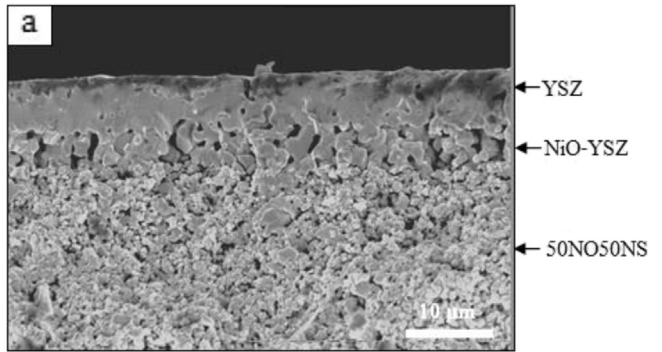


Fig. 6. Fractured surfaces of (a) 50NO50NS-3, (b) 55NO45NS-3 and (c) 60NO40NS-3 cells.

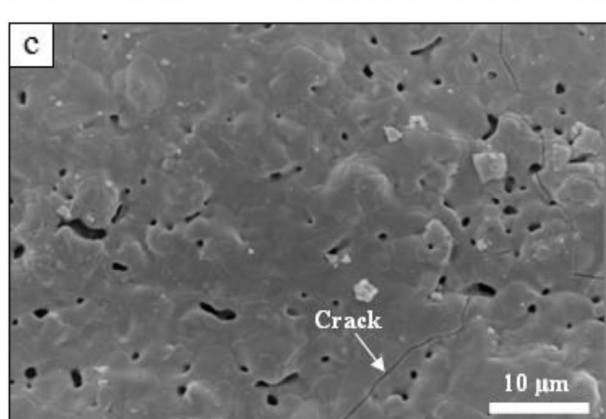
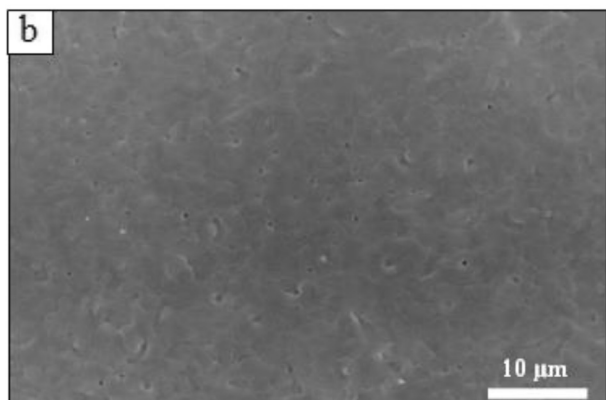
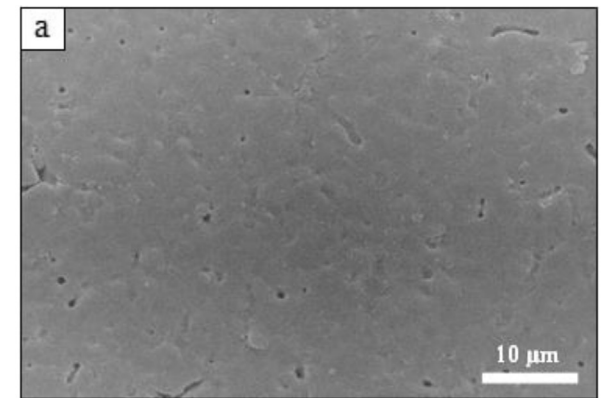


Fig. 7. Surfaces of YSZ electrolyte layers on (a) 50NO50NS-3, (b) 55NO45NS-3 and (c) 60NO40NS-3 cells.

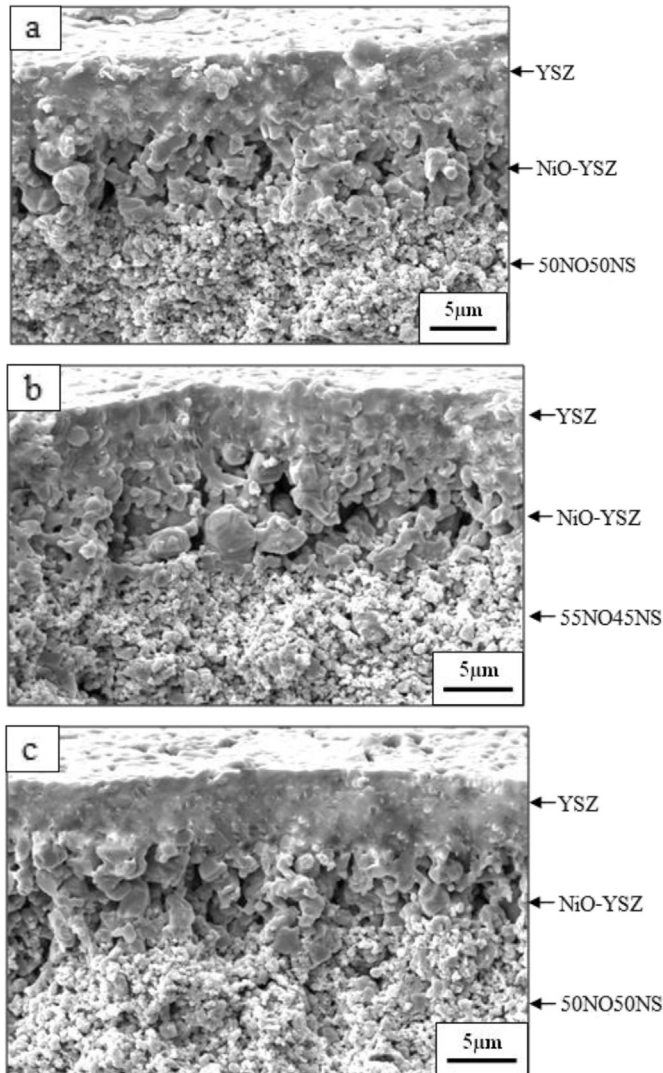


Fig. 8. Fractured surfaces of (a) 50NO50NS-1, (b) 55NO45NS-1 and (c) 60NO40NS-1 cells.

achieved in all cells. Especially, YSZ surface of 60NO40NS-3 cell (Fig. 9c) was obviously observed that pores were eliminated. Moreover, crack on YSZ layer was eliminated for 60NO40NS-1 cell, although TEC value of 60NO40NS support and YSZ electrolyte was still different.

The cell voltage and power density as a function of the current density for 50NO50NS-3, 55NO45NS-3 and 60NO40NS-3 cells were displayed in Fig. 10. The power density of 50NO50NS-3 cell was about 70.2 mW cm^{-2} while the highest power density (94.5 mW cm^{-2}) was received from 55NO45NS-3. This was probably due to the superior electrical conductivity of the 55NO45NS support to that of the 50NO50NS support (Fig. 6). The power density of only 43.3 mW cm^{-2} at 800°C was obtained from the 60NO40NS-3 cell, although the 60NO40NS support had the highest electrical conductivity. The inferior performance of this cell was possibly because of the high porosity and crack defects observed in the electrolyte layer. It was explained that the transportation of oxygen ion from anode was obstructed by crack and pore in YSZ electrolyte. This reason could be confirmed by the lowest OCV value (0.84 V) in Fig. 10.

The cell performance of the 50NO50NS-1, 55NO45NS-1 and 60NO40NS-1 cells is shown in Fig. 11. Power densities of cells were

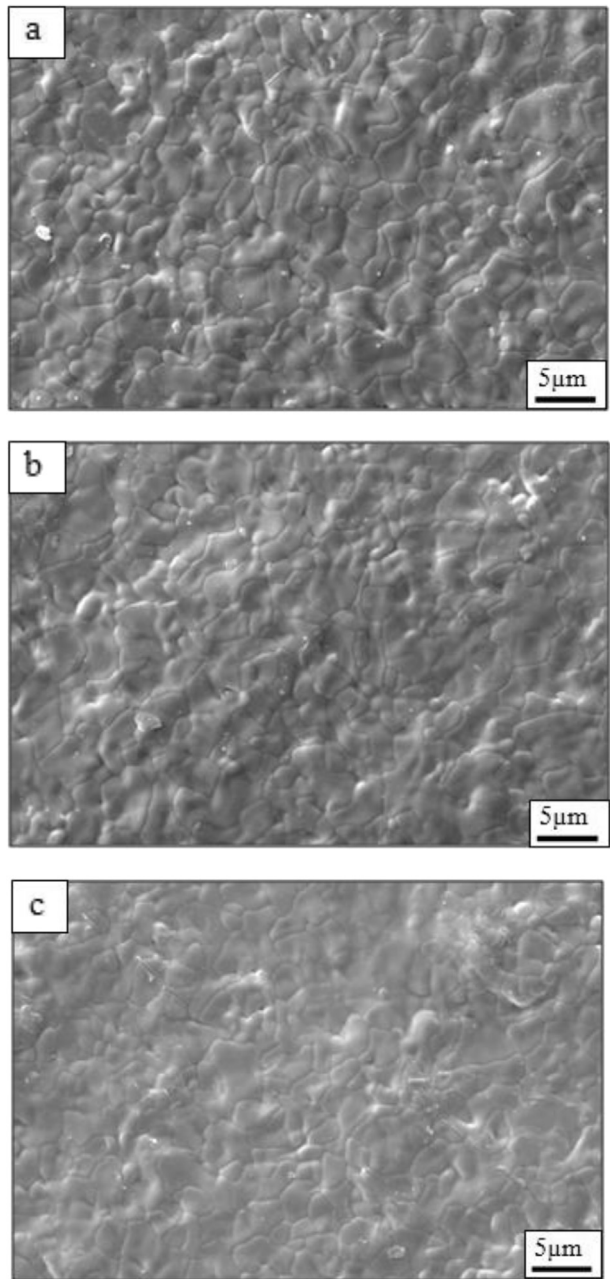


Fig. 9. Surfaces of YSZ electrolyte layers on (a) 50NO50NS-1, (b) 55NO45NS-1 and (c) 60NO40NS-1 cells.

enhanced with increasing Ni contents of the supports. It was explained that electrons could be easily conducted for the higher Ni metallic phase of supports resulting in lower ohmic polarization loss. In comparison of the cell with different firing rates, it was found that power density on the cells of 50NO50NS-1 (76.9 mW cm^{-2}), 55NO45NS-1 (95.6 mW cm^{-2}) and 60NO40NS-1 cell (105.9 mW cm^{-2}) increased when the firing rate was reduced from 3°C min^{-1} to 1°C min^{-1} (Fig. 11). This was probably due to an increase in the degree of densification of YSZ electrolyte layer leading to the improvement of ohmic loss and overall cell performance, which was confirmed by the lower slope of the linear part of the $I-V$ curve in Fig. 11. From above results, it was investigated that the optimum cell performance was obtained for 60NO40NS-1 cell because of the highest electrical conductivity of 60NO40NS, while dense electrolyte layer could be improved with the firing rate of

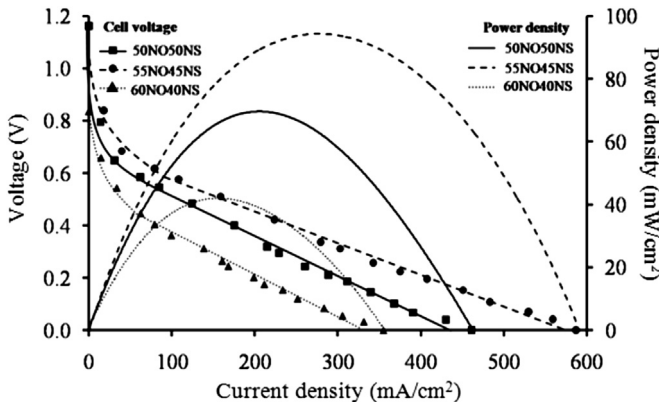


Fig. 10. Cell performance of the reduced single cells with the heating rate of $3\text{ }^{\circ}\text{C min}^{-1}$.

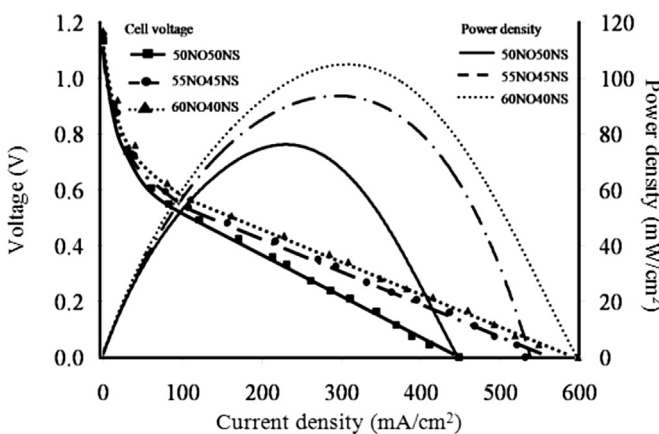


Fig. 11. Cell performance of the reduced single cells with the heating rate of $1\text{ }^{\circ}\text{C min}^{-1}$.

$1\text{ }^{\circ}\text{C min}^{-1}$. At high OCV value of cells, the current density seems limited, which was close to the research of Leng et al. for using Pt as the cathode. Their report explained that Pt cathode had high polarization resistance ($\sim 1.8\text{ }\Omega\text{ cm}^2$) at $800\text{ }^{\circ}\text{C}$ [16]. Besides, the only electronic phase of Pt cathode resulted in low electrochemical reaction at cathode side which affected on the increase of activation polarization loss.

Fig. 12 shows the durability of 60NO40NS-1 cell at constant voltage potential of 0.62 V. It was found that the current density of the cell was stable for 600 min. This result confirmed that the NiO–NiAl₂O₄ supported cell could endurance in H₂–O₂ system.

4. Conclusion

This research showed that NiO/NiAl₂O₄ with the NiO content between 50 and 60 wt.% was successfully used as an external supports for SOFCs. The results showed that successful fabrication of cell components depended on compatible shrinkage difference

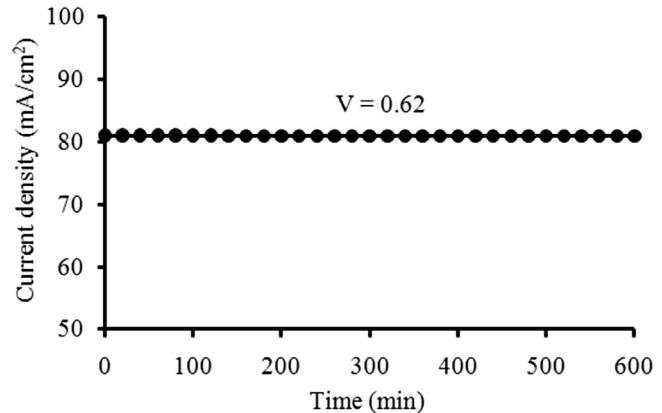


Fig. 12. The current density of 60NO40NS-1 cell with the time in H₂–O₂ system.

and TEC of the cell components with the type of supports. With a careful control of the firing scheme, high densification and crack-free electrolyte layers could be obtained. The power densities of the cells were then increased. Besides, the power density values of the cells were increased with higher Ni content in the supports due to an increase of Ni metallic connection. Further development of the cell configuration and design is still required in order to improve the cell performance to match with market requirement.

Acknowledgments

The financial support from Thailand Graduated Institute of Science and Technology (TGIST) and Mae Fah Luang University are highly appreciated.

References

- [1] J.M. Serra, V.B. Vert, O.B. Chler, W.A. Meulenbergh, H.P. Buchkremer, *Chem. Mater.* 20 (2008) 3867–3875.
- [2] N.Q. Minh, T. Takahashi, *Science and Technology of Ceramic Fuel Cells*, Applied Signal, Inc., California, USA, 1995, pp. 6–10.
- [3] S.C. Singhal, K. Kendall, *High Temperature Solid Oxide Fuel Cells: Fundamentals, Design and Applications*, Elsevier Ltd., Oxford, 2003, pp. 196–206.
- [4] J. Will, A. Mitterdorfer, C. Kleinlogel, D. Perednis, L.J. Gauckler, *Solid State Ionics* 131 (2000) 79–96.
- [5] M.C. Tucker, G.Y. Lau, C.P. Jacobson, L.C. DeJonghe, S.J. Visco, *J. Power Sources* 171 (2007) 477–482.
- [6] M.C. Tucker, G.Y. Lau, C.P. Jacobson, L.C. DeJonghe, S.J. Visco, *J. Power Sources* 175 (2008) 447–451.
- [7] M. Brandner, M. Bram, J. Froitzheim, H.P. Buchkremer, D. Stover, *Solid State Ionics* 179 (2008) 1501–1504.
- [8] S. Molin, M. Gazda, P. Jasinski, *Solid State Ionics* 181 (2010) 1214–1220.
- [9] P. Saltykov, O. Fabrichnaya, J. Golczewski, F. Aldinger, *J. Alloys Compd.* 381 (2004) 99–113.
- [10] N. Vivet, S. Chupin, E. Estrade, A. Richard, S. Bonnamy, D. Rochais, E. Bruneton, *J. Power Sources* 196 (2011) 9989–9997.
- [11] B.K. Kwak, H.K. Youn, J.S. Chung, *J. Power Sources* 185 (2008) 633–640.
- [12] C.G. Kuo, W.D. Jehng, S.J. Hsieh, C.C. Chen, *J. Alloys Compd.* 480 (2009) 299–305.
- [13] W.Z. Zhu, S.C. Deevi, *Mater. Sci. Eng. A* 362 (2003) 228–239.
- [14] G.B. Jung, K.F. Lo, S.H. Chan, *J. Solid State Electrochem.* 11 (2007) 1435–1440.
- [15] S. Molin, B. Kusz, M. Gazda, P. Jasinski, *J. Power Sources* 181 (2008) 31–37.
- [16] Y.J. Leng, S.H. Chan, K.A. Khor, S.P. Jiang, P. Cheang, *J. Power Sources* 117 (2003) 26–34.